
InCoM: Intent-Driven Perception and Structured Coordination for Whole-Body Mobile Manipulation

Jiahao Liu^{1,2} Wenbo Cui^{1,3} Haoran Li^{1,3} Dongbin Zhao^{1,3}

Abstract

Whole-body mobile manipulation is a fundamental capability for general-purpose robotic agents, requiring both coordinated control of the mobile base and manipulator and robust perception under dynamically changing viewpoints. However, existing approaches face two key challenges: strong coupling between base and arm actions complicates whole-body control optimization, and perceptual attention is often poorly allocated as viewpoints shift during mobile manipulation. We propose **InCoM**, an intent-driven perception and structured coordination framework for whole-body mobile manipulation. InCoM infers latent motion intent to dynamically reweight multi-scale perceptual features, enabling stage-adaptive allocation of perceptual attention. To support robust cross-modal perception, InCoM further incorporates a geometric–semantic structured alignment mechanism that enhances multimodal correspondence. On the control side, we design a decoupled coordinated flow matching action decoder that explicitly models coordinated base–arm action generation, alleviating optimization difficulties caused by control coupling. Without access to privileged perceptual information, InCoM outperforms state-of-the-art methods on three ManiSkill-HAB scenarios by **28.2%**, **26.1%**, and **23.6%** in success rate, demonstrating strong effectiveness for whole-body mobile manipulation.

1. Introduction

Whole-body mobile manipulation is a fundamental capability for realizing general-purpose robotic policies in real-

¹Institute of Automation, Chinese Academy of Science, Beijing, China ²School of Advanced Interdisciplinary Sciences, University of the Chinese Academy of Sciences, Beijing, China ³School of Artificial Intelligence, University of Chinese Academy of Sciences, Beijing, China. Correspondence to: Haoran Li <lihaoran2015@ia.ac.cn>, Dongbin Zhao <dongbin.zhao@ia.ac.cn>.

world environments and has attracted increasing attention from both academia and industry (Fu et al., 2024; Chen et al., 2025; Jiang et al., 2025; Su et al., 2025). Compared with tabletop manipulators or mobile bases, whole-body mobile manipulation requires the simultaneous control of both the robotic arm and the mobile base, and perform continuous decision-making and control in complex, dynamic, and partially observable environments (Yang et al., 2024; Uppal et al., 2024).

Generating stable coordinated actions between the mobile base and the manipulator is a key challenge for whole-body mobile manipulation. Due to inevitable execution errors in real robots, small deviations in base motion can be amplified at the end-effector of the manipulator with a decoupled or weakly coordinated manner (Jiang et al., 2025), leading to degraded manipulation accuracy or failure of the task. Introducing conditional dependencies between the mobile base and the manipulator at the action decoding stage (Chen et al., 2025; Jiang et al., 2025) can partially alleviate the above issues. However, such joint action modeling typically represents coordination as a one-way dependency, which limits the model’s ability to capture the bidirectional coupling and mutual compensation inherent in real-world tasks.

Another important yet often overlooked challenge in mobile manipulation is the allocation of perceptual information under dynamically changing viewpoints, which we refer to as the dynamic perceptual attention problem. Unlike single-mode settings such as tabletop manipulation or navigation, mobile manipulation involves the combination and switching of multiple operational modes, each with distinct perceptual requirements. For example, in a task such as *move a trash bin next to the bed* shown in Fig. 1, the policy must focus on the interaction location between the gripper and the rim of the trash bin to ensure a safe and reasonable grasp, whereas during navigation toward the bed, attention should shift to freespace and obstacle boundaries to avoid collisions. However, most existing end-to-end mobile manipulation policies (Zhao et al., 2023; Chi et al., 2024; Ze et al., 2024; Su et al., 2025) neglect this issue, making it difficult for the optimization process to capture the evolving perceptual demands as the task progresses. As a result, perceptual attention becomes dispersed during execution,

which ultimately degrades task success rates.

To address these challenges, we propose an end-to-end framework named InCoM for whole-body mobile manipulation that jointly considers stage-adaptive perception and coordinated whole-body action generation. The framework explicitly models the evolution of perceptual attention throughout task execution, while enabling stable and efficient generation of coordinated base–arm actions. Specifically, to address the dynamic perceptual attention problem induced by viewpoint changes, we propose a multi-scale perception architecture that infers the robot’s latent motion intent and dynamically allocates perceptual attention according to the current task stage, enabling adaptive fusion of global scene context and local detail cues. This design improves the model’s robustness to viewpoint changes induced by motion. In addition, to better integrate information across modalities, we introduce a cross-modal alignment and fusion module that models geometric consistency and semantic correspondence, thereby enhancing the efficiency and effectiveness of multimodal information fusion. Finally, to tackle the problem of joint action generation, we design an action generation mechanism that enables information interaction between the mobile base and the manipulator during decoding, allowing bidirectional coordination and mutual compensation. The main contributions of this work are summarized as follows:

- We propose InCoM, an end-to-end framework for whole-body mobile manipulation that jointly models intent-driven perception and coordinated action generation within a unified learning formulation, alleviating perceptual dispersion and control coupling in mobile manipulation.
- We design an Intent-Driven Pyramid Perception Module (IDPPM) that infers latent motion intent to adaptively reweight multi-scale perceptual features, enabling stage-aware allocation between global context and local fine-grained details. To enhance cross-modal alignment, we further propose a Dual-stream Affinity Refinement Module (DARM) that explicitly models and fuses geometric and semantic affinities.
- We introduce a Decoupled Coordinated Flow Matching (DCFM) decoder that explicitly captures bidirectional coordination between the mobile base and the manipulator, producing expressive whole-body actions.
- Without relying on privileged perceptual information, InCoM outperforms state-of-the-art methods on three ManiSkill-HAB (Shukla et al., 2025) scenarios by **28.2%**, **26.1%**, and **23.6%** in success rate, demonstrating strong effectiveness for whole-body mobile manipulation.

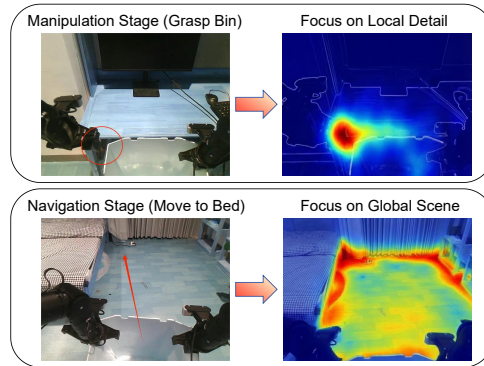


Figure 1. **Dynamic perceptual attention during the whole-body mobile manipulation.** The left half is the color image, and the right half is a schematic diagram of perceptual attention. During manipulation, perceptual attention is primarily focused on local interaction targets; for example, the agent should attend to whether the robotic arm has successfully grasped the trash bin(top). During navigation, perceptual attention shifts toward understanding the global structure to identify freespace (bottom).

2. Related Works

2.1. Whole-Body Mobile Manipulation Policies

Early mobile manipulation systems commonly decomposed tasks into base navigation and arm manipulation, coordinating the two components via phase-switching rules or high-level planners (Garrett et al., 2020; Ahn et al., 2022; Liu et al., 2024; Mao et al., 2025; Qiu et al., 2025). While effective in structured settings, such modular designs often suffer from motion discontinuities and error accumulation when task phases are tightly coupled or environments become dynamic. To address these limitations, recent research has increasingly shifted toward end-to-end imitation learning frameworks that jointly model whole-body actions. Existing work adopts a variety of action modeling strategies, including chunk-wise sequence modeling with Transformers (Zhao et al., 2023), multi-modal fusion of visual observations for joint action prediction (Su et al., 2025), and generative trajectory modeling using diffusion processes (Yan et al., 2025). These methods improve temporal coherence and reduce hand-designed coordination rules, yet most treat the mobile base and the manipulator as a unified action vector, without explicitly modeling their mutual dependencies. The vision–language–action (VLA) methods (Brohan et al., 2023; Team et al., 2024; Kim et al., 2024; 2025) further enhance generalization by leveraging large-scale pretraining. However, existing VLA-based systems primarily focus on tabletop manipulation, and thus do not fully capture the dependencies between movement and manipulation in mobile manipulation tasks. BEHAVIOR Robot Suite (Jiang et al., 2025) partially addresses this issue by adopting a hierarchical diffusion decoding strategy to model conditional dependencies between the base and the arm, while AC-DiT (Chen et al., 2025) introduces a

mobility-to-body conditioning mechanism that modulates whole-body action generation using mobility-related context. Nevertheless, their unidirectional modeling strategies still struggle to reflect the reciprocal coordination commonly observed in real-world whole-body interactions. In contrast, our work explicitly models bidirectional coordination between the mobile base and the manipulator within an end-to-end framework, aiming to improve both action coherence and execution stability.

2.2. Multi-Modal and Multi-Scale Visual Perception

Whole-body mobile manipulation exhibits stage-dependent perceptual requirements (Chen et al., 2025), where navigation emphasizes global scene understanding while interaction demands fine-grained local perception. This has motivated growing interest in multi-modal and multi-scale visual representations. Pretrained 2D visual models provide strong 2D semantic cues (Radford et al., 2021; Oquab et al., 2024; Tschannen et al., 2025), whereas 3D perception methods capture spatial structure and object geometry (Choy et al., 2019; Jia et al., 2024; Wu et al., 2024), offering complementary information for robust manipulation. Several works (Chen et al., 2025) attempt to balance these cues via adaptive weighting mechanisms across modalities, yet typically operate on fixed-scale perceptual representations, limiting the ability to adapt perceptual granularity as tasks progress. In contrast, extensive evidence from computer vision indicates that multi-scale feature representations are critical for complex scene understanding: features at different depths naturally specialize in distinct perceptual scopes, with shallow layers capturing local details and deeper layers encoding global context (Jiang et al., 2024). Despite their success in object detection and scene parsing (Lin et al., 2017; Chen et al., 2017; Zhao et al., 2017; Qi et al., 2017; Liu et al., 2021; Schult et al., 2023), such multi-scale scheduling remains underexplored in mobile manipulation.

Cross-modal fusion requires establishing accurate correspondence between 3D point cloud representations (e.g., voxels) and 2D image features (e.g., patches). Early projection-based approaches (Vora et al., 2020) rely on implicit correspondence learning through geometric projection, but are highly sensitive to calibration errors and projection noise. More recent Transformer-based methods employ cross-attention (Bai et al., 2022) or 3D positional embeddings (Liu et al., 2022; Su et al., 2025) to implicitly model 2D–3D alignment, alleviating the need for explicit projection rules. Deformable attention mechanisms further introduce local adaptivity to refine fine-grained correspondences and mitigate context misalignment (Cui et al., 2025), but often rely on large-scale domain-specific pretraining to achieve stable performance. By contrast, the proposed DARM module explicitly models geometric affinity and semantic affinity in parallel during cross-modal fusion, de-

coupling spatial correspondence reasoning from semantic matching. This enables adaptive balancing of geometric consistency and semantic relevance without large-scale pre-training, improving robustness in cross-modal alignment.

3. Methodology

3.1. Problem Formulation and Overall Framework

Whole-body mobile manipulation can be modeled as a discrete-time partially observable Markov decision process (POMDP). At time step t , the robot receives an observation $\mathcal{O}_t = \{P_t, \mathcal{I}_t, \mathbf{s}_t\}$, where P_t denotes a sparse 3D point cloud, $\mathcal{I}_t = \{I_t^v\}_{v=1}^V$ represents multi-view RGB images, and \mathbf{s}_t is the proprioceptive state, including joint positions, joint velocities, and end-effector poses. The action space is explicitly factorized into two subspaces corresponding to mobility and manipulation: $\mathbf{a}_t = [\mathbf{a}_t^{base}, \mathbf{a}_t^{arm}] \in \mathcal{A}$, where $\mathbf{a}_t^{base} \in \mathbb{R}^{d_{base}}$ controls the linear and angular velocities of the mobile base, while $\mathbf{a}_t^{arm} \in \mathbb{R}^{d_{arm}}$ controls the arm joints and the gripper. Our objective is to learn a conditional policy $\pi_\theta(\mathbf{a}_{t:t+T_p} | \mathcal{O}_t, \mathbf{a}_{t-H:t-1})$, which generates a coordinated whole-body action sequence over the next T_p time steps, conditioned on the current observation and a history of past actions $\mathbf{a}_{t-H:t-1}$.

We introduce a unified framework for whole-body mobile manipulation named InCoM. As shown in Fig. 2, InCoM comprises three core components: an Intent-Driven Pyramid Perception Module (IDPPM), a Dual-stream Affinity Refinement Module (DARM), and a Decoupled Coordinated Flow Matching (DCFM) decoder. Multi-modal observations are first encoded into a multi-scale feature pyramid. At each scale, DARM jointly models geometric and semantic affinities between point cloud and image features to produce aligned cross-modal representations. IDPPM then infers implicit motion intent from historical actions and global context, and adaptively reweights features across scales to enable stage-aware perception allocation. The aggregated features are finally decoded by DCFM to generate coordinated whole-body actions for the mobile base and manipulator.

3.2. Intent-Driven Pyramid Perception Module

In whole-body mobile manipulation tasks, the mobile base and the manipulator require perceptual information with different spatial coverage and resolution across task stages. Existing mobile manipulation policies (Chen et al., 2025; Su et al., 2025; Jiang et al., 2025) typically adopt fixed-scale perception encoders, which struggle to jointly support global scene understanding and local fine-grained modeling as navigation and precise manipulation alternate. To address this limitation, we propose IDPPM (Intent-Driven Pyramid Perception Module), a pyramid-based perceptual module

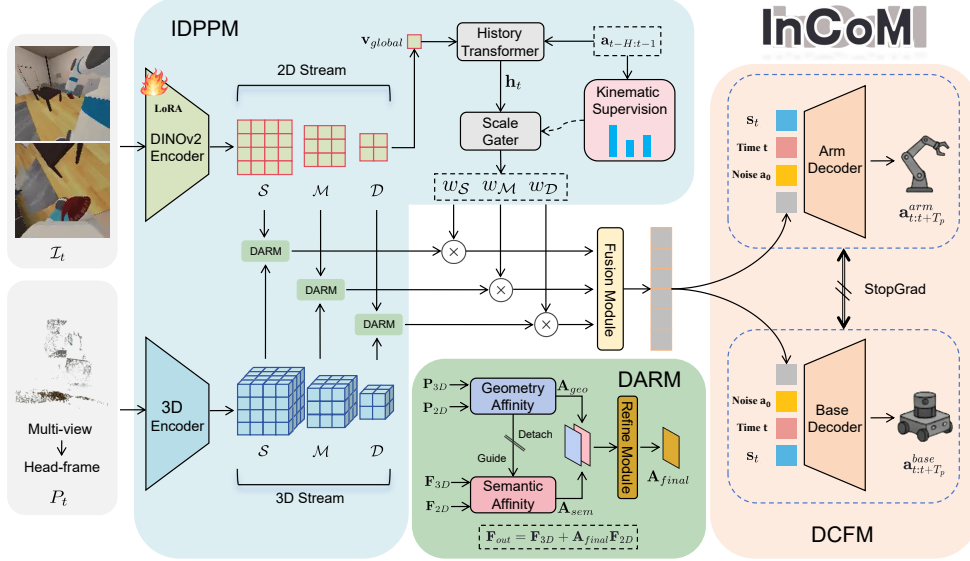


Figure 2. **Overview of InCoM.** The framework integrates intent-driven multi-scale perception (IDPPM), dual-stream cross-modal affinity refinement (DARM), and decoupled flow-based action generation (DCFm) to produce coordinated whole-body mobile manipulation.

that dynamically reweights multi-scale features using historical actions and global visual context, enabling adaptive allocation of perceptual information across levels.

Hierarchical Feature Pyramid. We extract features using a sparse 3D encoder (Choy et al., 2019) and a pretrained 2D visual encoder (DINOv2 (Oquab et al., 2024)), and align them across three abstraction levels $k \in \{S, M, D\}$. At the shallow level, high-resolution point cloud features are aligned with local detail information extracted from the shallow layers of DINOv2, primarily to support fine-grained manipulation tasks such as object grasping; meanwhile, at the mid level, point cloud features with a spatial receptive field intermediate between local and global scales are aligned with the mid-level features of DINOv2, serving to bridge local detail information and global scene understanding; and finally, at the deep level, point cloud features that represent large-scale spatial structure are aligned with the global scene features from the final layer of DINOv2, primarily to support mobile base navigation.

Intent Modulation. To dynamically allocate perceptual attention according to task stages, we introduce a History Transformer, which maps the historical action sequence $\mathbf{a}_{t-H:t}$ together with the current global visual feature \mathbf{v}_{global} into an implicit intent vector \mathbf{h}_t . Here, \mathbf{v}_{global} corresponds to the classification token feature extracted from the final layer of DINOv2 (Oquab et al., 2024). Subsequently, an MLP-based ScaleGater network ϕ maps \mathbf{h}_t to a set of normalized hierarchical weights \mathbf{w}_t :

$$\mathbf{w}_t = [w_S, w_M, w_D] = \text{Softmax}(\phi(\mathbf{h}_t)) \quad (1)$$

Auxiliary Kinematic Supervision. To ensure consistency between the robot’s perceptual focus and its kinematic

state across different manipulation stages, we introduce a kinematics-guided loss function to regularize and reinforce the rationality of feature allocation. Specifically, we quantify the activity levels of the mobile base and the manipulator by computing the L_2 norms of their respective action increments over the historical action sequence:

$$I_{base} = \frac{1}{T_h} \sum_t \|\Delta \mathbf{a}_t^{base}\|_2, \quad I_{arm} = \frac{\alpha}{T_h} \sum_t \|\Delta \mathbf{a}_t^{arm}\|_2 \quad (2)$$

where α denotes a balancing coefficient. The target weight distribution \mathbf{w}^* is defined as:

$$w_D^* \propto I_{base}, \quad w_S^* \propto I_{arm}, \quad w_M^* \propto \sqrt{w_S^* w_D^*} \quad (3)$$

By minimizing the KL divergence $\mathcal{L}_{scale} = D_{KL}(\mathbf{w}_t || \mathbf{w}_t^*)$ the model learns to emphasize deep, global features during rapid motion and to focus on shallow, local features during fine-grained manipulation. In addition, to prevent the module from overfitting to rigid kinematic variations, we further introduce an entropy regularization term:

$$\mathcal{L}_{scale} = D_{KL}(\mathbf{w}_t || \mathbf{w}_t^*) + \lambda_{ent} \cdot \sum_{k \in \{S, M, D\}} w_k \log w_k \quad (4)$$

3.3. Dual-stream Affinity Refinement Module

Cross-modal alignment requires both geometric consistency and semantic correspondence with the color image and point cloud as the input. Existing methods (Su et al., 2025) often entangle geometric positional information and semantic features within a single attention computation, despite their differing statistical properties and stability. To address this issue, we propose a Dual-stream Affinity Refinement Module (DARM), which models geometric affinity and semantic

affinity in separate streams and fuses them via a lightweight mechanism, preserving spatial geometric constraints while maintaining discriminative semantic matching during cross-modal alignment.

Dual-Stream Affinity Modeling. Let the input consists of N 3D point-cloud voxels and M 2D image patches, where $M = V \times H \times W$ denotes the total number of patches across V views. $\mathbf{F}_{3D} \in \mathbb{R}^{N \times D}$ represents the feature vectors of 3D voxels, and $\mathbf{P}_{3D} \in \mathbb{R}^{N \times D}$ denotes their positional encodings obtained from 3D spatial coordinates. $\mathbf{F}_{2D} \in \mathbb{R}^{M \times D}$ represents the feature vectors of 2D image patches, and $\mathbf{P}_{2D} \in \mathbb{R}^{M \times D}$ denotes the corresponding composite positional embeddings, constructed by summing a fixed sinusoidal positional embedding \mathbf{P}_{sin} and a learnable view embedding \mathbf{E}_{view} , i.e., $\mathbf{P}_{2D} = \mathbf{P}_{sin} + \mathbf{E}_{view}$. To explicitly differentiate the roles of spatial geometry and appearance semantics in cross-modal alignment, we construct two affinity computation paths in parallel.

Geometric affinity \mathbf{A}_{geo} is computed from positional encodings of 3D voxels and 2D patches to capture cross-modal geometric consistency, while semantic affinity \mathbf{A}_{sem} is derived from high-dimensional feature representations to model appearance and semantic correspondence. Both affinities are implemented via scaled dot-product attention in distinct representation spaces, enabling decoupled modeling of geometric and semantic relationships. The resulting affinity maps are concatenated and adaptively fused through a lightweight 1×1 convolutional module f_{refine} to produce the final cross-modal attention distribution.

Geometry-Guided Attention Regularization. To further exploit the stability of geometric information during optimization, we treat the geometric affinity as a soft geometric consistency constraint that regularizes the search space of semantic matching. Specifically, the geometric affinity \mathbf{A}_{geo} is normalized via Softmax to construct a transport cost matrix $\mathbf{C} = \mathbf{1} - \text{Softmax}(\mathbf{A}_{geo})$, where a smaller value of \mathbf{C}_{ij} indicates higher similarity between voxel i and patch j in the geometric positional embedding space. Based on this cost matrix, we apply the Sinkhorn–Knopp algorithm to compute a joint probability distribution $\mathbf{T}^* \in \mathbb{R}^{N \times M}$ that satisfies geometric consistency preferences. This distribution serves as a soft geometric reference that characterizes physically plausible cross-modal matching regions under the current observation. We then minimize the KL divergence between the semantic attention distribution $\mathbf{P}_{sem} = \text{Softmax}(\mathbf{A}_{sem})$ and $\mathbf{T}^* \in \mathbb{R}^{N \times M}$, thereby encouraging semantic matching to globally respect geometric consistency constraints:

$$\mathcal{L}_{align} = D_{KL}(\mathbf{P}_{sem} \parallel \text{sg}(\mathbf{T}^*)) \quad (5)$$

where $\text{sg}(\cdot)$ denotes the stop-gradient operator. This formulation decouples the optimization of the geometric and semantic branches, allowing geometric affinity to act as

a fixed prior for semantic attention, while preventing semantic noise from propagating back into geometric affinity modeling.

3.4. Decoupled Coordinated Flow Matching

Whole-body control tasks involve a fundamental tension between high-dimensional action spaces and cross-part coordination. Existing methods (Chen et al., 2025; Jiang et al., 2025) typically rely on unidirectional dependency modeling (e.g., conditioning the manipulator on the base), which fails to capture bidirectional interactions among body parts. To overcome this limitation, we propose DCFM (Decoupled Coordinated Flow Matching), a decoupled generative and explicitly coordinated whole-body action decoding framework shown in Fig. 3. DCFM adopts conditional flow matching instead of diffusion models to reduce iterative sampling overhead while improving action smoothness and stability.

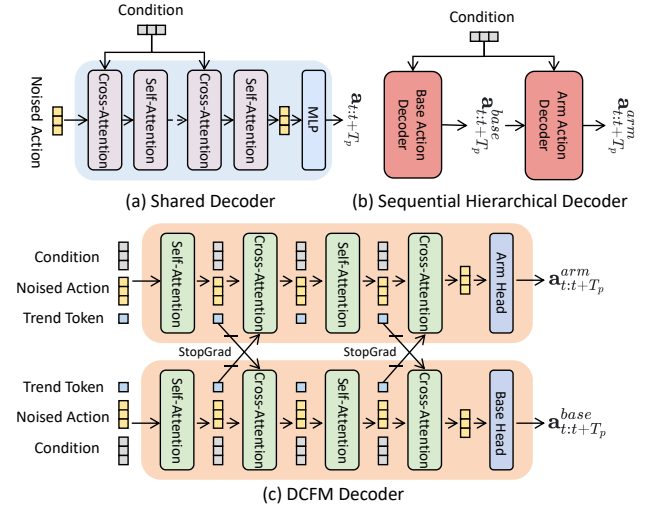


Figure 3. Comparison of the Action Decoders. (a) Shared Decoder: base and arm actions are jointly modeled by a single decoder with a unified output head. (b) Sequential Hierarchical Decoder: base and arm actions are predicted by independent decoders, where the arm decoder is conditioned on the base output, capturing only unidirectional dependency. (c) DCFM Decoder: base and arm actions are decoded in parallel and exchange information bidirectionally via cross-attention in intermediate layers. To avoid unstable gradient interference during training, stop-gradient is applied in the cross-attention, retaining only forward conditional information.

Decoupled Generation Architecture. We first explicitly factorize the high-dimensional whole-body action space into the base actions \mathbf{a}^{base} and the arm actions \mathbf{a}^{arm} . To avoid the error accumulation and computational overhead associated with diffusion models, we construct a direct linear path between a noise distribution $\mathbf{a}_0 \sim \mathcal{N}(\mathbf{0}, \mathbf{I})$ and the expert action distribution \mathbf{a}_1 :

$$\mathbf{a}_t = (1 - t)\mathbf{a}_0 + t\mathbf{a}_1, \quad t \in [0, 1] \quad (6)$$

Along this path, the flow velocity is constant and defined as $\mathbf{u} = \mathbf{a}_1 - \mathbf{a}_0$. Consequently, our network v_θ only needs to learn to predict this constant velocity vector. Separate Transformer decoders are trained for the mobile base and the manipulator, respectively, to minimize the prediction error:

$$\mathcal{L}_{flow} = \sum_{k \in \{base, arm\}} \|v_\theta^k(\mathbf{a}_t^k, t, c) - (\mathbf{a}_1^k - \mathbf{a}_0^k)\|^2 \quad (7)$$

where c denotes the conditioning embedding defined as $c = \psi(\mathcal{O}_t, \mathbf{a}_{t-H:t-1})$. Here, ψ is a multimodal feature fusion network that aggregates the current point cloud, images, proprioceptive state, and historical action sequence into a unified context representation.

Explicit Bidirectional Coordination. While decoupled generation alleviates the dimensionality challenge, it overlooks physical coupling between body parts. To address this, we introduce an information interaction mechanism between the two generation streams. As shown in Fig. 3(c), each decoder branch maintains a learnable trajectory summary token that aggregates predicted motion trends, and at each Transformer layer, the mobile base and the manipulator exchange this information via cross-attention with stop-gradient to ensure bidirectional coordination.

3.5. Overall Optimization Objective

The final training objective is a weighted combination of the flow matching loss, the auxiliary kinematic supervision, and the geometry-guided attention regularization:

$$\mathcal{L}_{total} = \mathcal{L}_{flow} + \lambda_{scale}\mathcal{L}_{scale} + \lambda_{align}\mathcal{L}_{align} \quad (8)$$

4. Experiments

We systematically evaluate the effectiveness of the InCoM framework in whole-body mobile manipulation tasks. First, in Section 4.1, we conduct experiments on three different mobile manipulation scenarios in the ManiSkill-HAB (Shukla et al., 2025) simulation platform: SetTable, TidyHouse, and PrepareGroceries. The results show that InCoM consistently outperforms existing state-of-the-art baselines in terms of task success rates. Next, in Section 4.2, we perform a comprehensive ablation study to assess the contribution and necessity of each component of InCoM. Finally, Section 4.3 presents a visual analysis of the multi-scale modulation weights of IDPPM during task execution, further confirming the effectiveness and rationale of the modulation mechanism.

4.1. ManiSkill-HAB Evaluation

4.1.1. EVALUATION SETTINGS

To evaluate robustness under realistic sensing constraints, we modify the standard observation space of ManiSkill-HAB (Shukla et al., 2025) by removing simulator-privileged signals. While the original environment provides high-precision state information such as target object pose and grasp indicators in addition to RGB, depth, and robot proprioception, such information is typically unavailable in real-world settings. Our setup *excludes these privileged observations*, requiring the agent to *rely solely on visual inputs and basic proprioceptive feedback* to infer object locations and grasp success, thereby substantially increasing task difficulty.

Baseline Methods. We compare InCoM with several representative mobile manipulation baselines. DP (Chi et al., 2024) and ACT (Zhao et al., 2023) adopt end-to-end policies with RGB and depth observations for joint action prediction, while DSPv2 (Su et al., 2025) leverages RGB images and point cloud inputs. WB-VIMA (Jiang et al., 2025) employs a hierarchical action decoder designed for whole-body manipulation and uses relatively sparse colored point clouds as perceptual input. AC-DiT (Chen et al., 2025) uses RGB images, point clouds, and language instructions with a mobility-to-body conditioning mechanism. Since its implementation is not publicly available, we directly report the results from the original paper, which are obtained under settings with access to privileged information, such as target object pose and grasp success signals. We additionally provide a separate comparison with a large-scale pretrained model, π_0 , in Appendix A.

4.1.2. SETTABLE SCENARIO

In this scenario, the robot must coordinate its mobile base and manipulator to open closed drawer and fridge, move bowl and apple from inside onto a dining table, and then close the drawer and fridge. This task involves the most diverse set of skills and explicitly tests the robot’s capability in handling articulated objects.

SetTable Scenario Results. All visualization trajectories are provided in Appendix A. Table 1 summarizes the quantitative results. InCoM achieves the highest success rates on most tasks and consistently outperforms all baselines on average, demonstrating strong whole-body mobile manipulation capability under perception-limited settings. DP, ACT, and DSPv2 exhibit notably lower success rates on pick-type tasks, suggesting limitations in precise object localization and fine-grained interaction when operating with dynamic viewpoints. WB-VIMA incorporates a hierarchical action decoder tailored for mobile manipulation; however, its performance remains constrained by insufficient

Table 1. Task success rate comparison on the SetTable scenario in the ManiSkill-HAB benchmark.

Method	Pick Apple	Place Apple	Open Fridge	Pick Bowl	Place Bowl	Open Drawer	Close Drawer	Mean
DP (Chi et al., 2024)	0.5	54.5	63.0	2.1	63.5	5.3	89.4	39.8
ACT (Zhao et al., 2023)	1.6	21.2	74.6	9.0	21.7	48.1	91.5	38.2
WB-VIMA (Jiang et al., 2025)	1.6	57.7	27.0	1.6	60.3	5.3	87.3	34.4
DSPv2 (Su et al., 2025)	1.4	65.2	73.4	1.4	85.7	29.9	98.4	50.8
AC-DiT (Chen et al., 2025)	33.3	33.3	90.7	36.0	17.3	81.3	97.3	55.6
InCoM(Ours)	59.4	84.1	87.3	84.1	82.5	88.9	100	83.8

perceptual modeling, particularly under dynamic attention requirements. Notably, AC-DiT, despite access to privileged state information, is still outperformed by InCoM overall, highlighting the effectiveness of intention-driven perception and coordinated action generation in challenging mobile manipulation scenarios.

4.1.3. TIDYHOUSE SCENARIO

In this scenario, the robot must pick and place nine different target objects onto designated open containers, such as tabletops or countertops. This scenario contains the largest variety of object categories among all experimental settings and is trained under a multi-task joint learning setup, which tests the model’s fine-grained perception of small objects as well as its ability to generalize and share decisions across different object categories and placement targets.

Table 2. Task success rate comparison on the TidyHouse scenario in the ManiSkill-HAB benchmark.

Method	Pick All	Place All	Mean
DP (Chi et al., 2024)	0	30.3	15.2
ACT (Zhao et al., 2023)	2.2	31.6	16.9
WB-VIMA (Jiang et al., 2025)	0.8	29.4	15.1
DSPv2 (Su et al., 2025)	1.3	42.1	21.7
InCoM(Ours)	16.7	78.9	47.8

TidyHouse Scenario Results. Table 2 summarizes the quantitative evaluation of different methods in the TidyHouse scenario. InCoM achieves the highest success rates in both pick-all and place-all tasks, with an average success rate of 47.8%, substantially higher than the second-best method DSPv2 (21.7%). In contrast, DP, ACT, and WB-VIMA show near-zero success rates in pick-all tasks, and DSPv2, while improved in place-all, still performs poorly on pick-all. These results indicate that InCoM maintains more stable performance across multiple-object manipulation tasks, with significantly smaller performance degradation as task complexity increases.

4.1.4. PREPAREGROCERIES SCENARIO

In this scenario, the robot must pick objects from the fridge and place them onto a countertop, and subsequently return the objects from the countertop back into the fridge. The

task involves complex obstacle avoidance and evasive maneuvers, and requires the robot to perform stable and precise interactions within confined and enclosed spaces.

Table 3. Task success rate comparison on the PrepareGroceries scenario in the ManiSkill-HAB benchmark.

Method	Pick All	Place All	Mean
DP (Chi et al., 2024)	0.4	17.7	9.1
ACT (Zhao et al., 2023)	2.0	27.5	14.8
WB-VIMA (Jiang et al., 2025)	0.8	22.0	11.4
DSPv2 (Su et al., 2025)	0.9	32.8	16.9
InCoM(Ours)	15.0	65.9	40.5

PrepareGroceries Scenario Results. Table 3 presents the results in the PrepareGroceries scenario, where the robot must move objects between the fridge and the countertop within a constrained space. InCoM consistently outperforms all baselines in both pick and place tasks, achieving an average success rate of 40.5% and a place-all success rate of 65.9%. DP, ACT, and WB-VIMA achieve near-zero pick success, and DSPv2 performs better on place-all but still below InCoM. This demonstrates that InCoM achieves higher overall task completion rates and maintains stable performance under increased task complexity and environmental constraints.

4.2. Ablation Study

As summarized in Table 4, we evaluate the contribution of each component by replacing it with a simpler or commonly used alternative while keeping the rest of the framework unchanged. Removing IDPPM and using a single-scale perceptual encoder leads to the largest performance drop, highlighting the critical role of multi-scale perception in handling stage-dependent sensing requirements for whole-body mobile manipulation. Replacing the adaptive scale weighting in IDPPM with a fixed multi-scale fusion results in a smaller but noticeable decrease, indicating that multi-scale features form the core perceptual representation, while intent-driven reweighting mainly optimizes their utilization across task stages. Substituting DARM with the Q-Former module from DSPv2 (Su et al., 2025) consistently reduces performance, demonstrating that explicitly separating and refining geometric and semantic affinities yields more robust cross-modal alignment than unified query-based fusion. Fi-

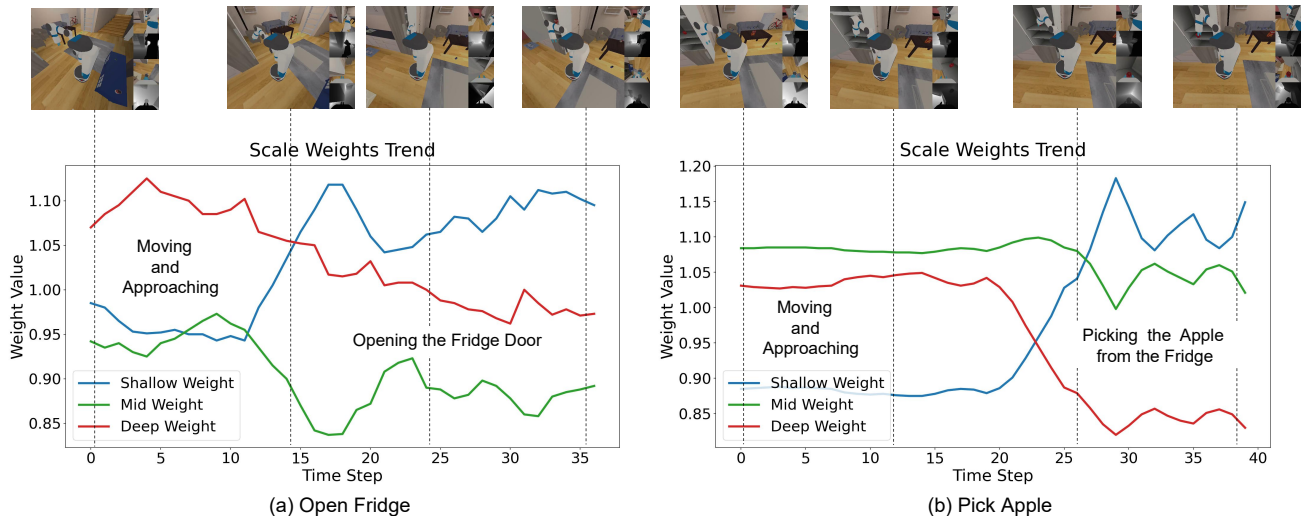


Figure 4. Variation of multi-scale modulation weights in the IDPPM during task execution.

nally, replacing DCFM with the dense head from DSPv2 (Su et al., 2025) also degrades performance, confirming that modeling coordinated whole-body action generation via conditional flow matching is essential for stable base–arm coordination.

Table 4. Ablation study of InCoM components.

Method	Mean Success Rate	Δ
InCoM (Full)	83.8	-
w/o IDPPM	64.3	↓ 19.5
w/o Weights	78.2	↓ 5.6
w/o DARM	77.6	↓ 6.2
w/o DCFM	75.9	↓ 7.9

4.3. Multi-scale Modulation Weight Analysis

Fig. 4 illustrates the dynamic evolution of the three levels of modulation weights within the IDPPM during mobile manipulation task execution. By analyzing the temporal progression of these weights, we can intuitively observe how the system autonomously adjusts its perceptual focus in response to latent motion intent.

As shown in Fig. 4(a,b), during the early stage of the task, the robot mainly executes base motions to approach the target, where deep-level features receive higher weights. This aligns with the design intuition that global scene representations are more critical at this stage for safe navigation and coarse motion planning. As the robot nears the target and transitions into the grasping phase, the weights progressively shift toward shallow-level features, indicating a change in perceptual focus. This behavior shows that IDPPM increasingly emphasizes fine-grained local details, which are essential for precise end-effector control, such as

object boundary alignment and contact reasoning.

5. Conclusion

We introduce InCoM, an end-to-end approach for whole-body mobile manipulation that addresses two key challenges: stage-dependent perceptual focus under dynamic viewpoints and coordinated action generation between the mobile base and the manipulator. By leveraging IDPPM, InCoM dynamically allocates multi-scale perceptual resources based on inferred motion intent, enabling the policy to adapt its sensing focus across navigation and manipulation stages. Through DARM, InCoM performs parallel geometric and semantic affinity modeling with adaptive fusion, resulting in more stable and reliable cross-modal alignment. Finally, DCFM enables coordinated whole-body action generation by explicitly modeling bidirectional interactions between the base and the arm through conditional flow matching. Evaluations on SetTable, TidyHouse, and PrepareGroceries without privileged information show that InCoM consistently outperforms existing methods, achieving higher task success rates and more stable whole-body motions in complex environments.

While InCoM achieves strong performance in whole-body mobile manipulation, several limitations remain. Training from scratch on task-specific data may limit generalization to unseen action modes or object interactions; incorporating large-scale pretrained representations and stronger reasoning mechanisms could improve adaptability. The current intent inference module, while effective, leaves room for improvement in modeling complex and rapidly evolving task dynamics, which may benefit from richer multi-step context or auxiliary supervision. In addition, extending the framework to long-horizon tasks is an interesting direction for future work.

Impact Statement

This paper presents work whose goal is to advance the field of machine learning. There are many potential societal consequences of our work, none of which we feel must be specifically highlighted here.

References

- Ahn, M., Brohan, A., Brown, N., Chebotar, Y., Cortes, O., David, B., Finn, C., Fu, C., Gopalakrishnan, K., Hausman, K., Herzog, A., Ho, D., Hsu, J., Ibarz, J., Ichter, B., Irpan, A., Jang, E., Ruano, R. J., Jeffrey, K., Jesmonth, S., Joshi, N. J., Julian, R., Kalashnikov, D., Kuang, Y., Lee, K.-H., Levine, S., Lu, Y., Luu, L., Parada, C., Pastor, P., Quiambao, J., Rao, K., Rettinghouse, J., Reyes, D., Sermanet, P., Sievers, N., Tan, C., Toshev, A., Vanhoucke, V., Xia, F., Xiao, T., Xu, P., Xu, S., Yan, M., and Zeng, A. Do as i can, not as i say: Grounding language in robotic affordances, 2022. URL <https://arxiv.org/abs/2204.01691>.
- Bai, X., Hu, Z., Zhu, X., Huang, Q., Chen, Y., Fu, H., and Tai, C.-L. Transfusion: Robust lidar-camera fusion for 3d object detection with transformers, 2022. URL <https://arxiv.org/abs/2203.11496>.
- Black, K., Brown, N., Driess, D., Esmail, A., Equi, M., Finn, C., Fusai, N., Groom, L., Hausman, K., Ichter, B., Jakubczak, S., Jones, T., Ke, L., Levine, S., Li-Bell, A., Mothukuri, M., Nair, S., Pertsch, K., Shi, L. X., Tanner, J., Vuong, Q., Walling, A., Wang, H., and Zhilinsky, U. π_0 : A vision-language-action flow model for general robot control, 2024. URL <https://arxiv.org/abs/2410.24164>.
- Brohan, A., Brown, N., Carbajal, J., Chebotar, Y., Chen, X., Choromanski, K., Ding, T., Driess, D., Dubey, A., Finn, C., Florence, P., Fu, C., Arenas, M. G., Gopalakrishnan, K., Han, K., Hausman, K., Herzog, A., Hsu, J., Ichter, B., Irpan, A., Joshi, N., Julian, R., Kalashnikov, D., Kuang, Y., Leal, I., Lee, L., Lee, T.-W. E., Levine, S., Lu, Y., Michalewski, H., Mordatch, I., Pertsch, K., Rao, K., Reymann, K., Ryoo, M., Salazar, G., Sanketi, P., Sermanet, P., Singh, J., Singh, A., Soricut, R., Tran, H., Vanhoucke, V., Vuong, Q., Wahid, A., Welker, S., Wohlhart, P., Wu, J., Xia, F., Xiao, T., Xu, P., Xu, S., Yu, T., and Zitkovich, B. Rt-2: Vision-language-action models transfer web knowledge to robotic control, 2023. URL <https://arxiv.org/abs/2307.15818>.
- Chen, L.-C., Papandreou, G., Kokkinos, I., Murphy, K., and Yuille, A. L. Deeplab: Semantic image segmentation with deep convolutional nets, atrous convolution, and fully connected crfs, 2017. URL <https://arxiv.org/abs/1606.00915>.
- Chen, S., Liu, J., Qian, S., Jiang, H., Li, L., Zhang, R., Liu, Z., Gu, C., Hou, C., Wang, P., Wang, Z., and Zhang, S. Ac-dit: Adaptive coordination diffusion transformer for mobile manipulation, 2025. URL <https://arxiv.org/abs/2507.01961>.
- Chi, C., Xu, Z., Feng, S., Cousineau, E., Du, Y., Burchfiel, B., Tedrake, R., and Song, S. Diffusion policy: Visuomotor policy learning via action diffusion, 2024. URL <https://arxiv.org/abs/2303.04137>.
- Choy, C., Gwak, J., and Savarese, S. 4d spatio-temporal convnets: Minkowski convolutional neural networks, 2019. URL <https://arxiv.org/abs/1904.08755>.
- Cui, W., Zhao, C., Chen, Y., Li, H., Zhang, Z., Zhao, D., and Wang, H. Cl3r: 3d reconstruction and contrastive learning for enhanced robotic manipulation representations, 2025. URL <https://arxiv.org/abs/2507.08262>.
- Darcet, T., Oquab, M., Mairal, J., and Bojanowski, P. Vision transformers need registers, 2024. URL <https://arxiv.org/abs/2309.16588>.
- Fu, Z., Zhao, T. Z., and Finn, C. Mobile aloha: Learning bimanual mobile manipulation with low-cost whole-body teleoperation, 2024. URL <https://arxiv.org/abs/2401.02117>.
- Garrett, C. R., Chitnis, R., Holladay, R., Kim, B., Silver, T., Kaelbling, L. P., and Lozano-Pérez, T. Integrated task and motion planning, 2020. URL <https://arxiv.org/abs/2010.01083>.
- Gu, X., Pang, T., Du, C., Liu, Q., Zhang, F., Du, C., Wang, Y., and Lin, M. When attention sink emerges in language models: An empirical view, 2025. URL <https://arxiv.org/abs/2410.10781>.
- Jia, Y., Liu, J., Chen, S., Gu, C., Wang, Z., Luo, L., Lee, L., Wang, P., Wang, Z., Zhang, R., and Zhang, S. Lift3d foundation policy: Lifting 2d large-scale pretrained models for robust 3d robotic manipulation, 2024. URL <https://arxiv.org/abs/2411.18623>.
- Jiang, D., Liu, Y., Liu, S., Zhao, J., Zhang, H., Gao, Z., Zhang, X., Li, J., and Xiong, H. From clip to dino: Visual encoders shout in multi-modal large language models, 2024. URL <https://arxiv.org/abs/2310.08825>.
- Jiang, Y., Zhang, R., Wong, J., Wang, C., Ze, Y., Yin, H., Gokmen, C., Song, S., Wu, J., and Fei-Fei, L. BEHAVIOR robot suite: Streamlining real-world whole-body manipulation for everyday household activities. In *9th Annual Conference on Robot Learning*, 2025. URL <https://openreview.net/forum?id=v2KevjWScT>.

- Kim, M. J., Pertsch, K., Karamcheti, S., Xiao, T., Balakrishna, A., Nair, S., Rafailov, R., Foster, E., Lam, G., Sanketi, P., Vuong, Q., Kollar, T., Burchfiel, B., Tedrake, R., Sadigh, D., Levine, S., Liang, P., and Finn, C. Openvla: An open-source vision-language-action model, 2024. URL <https://arxiv.org/abs/2406.09246>.
- Kim, M. J., Finn, C., and Liang, P. Fine-tuning vision-language-action models: Optimizing speed and success, 2025. URL <https://arxiv.org/abs/2502.19645>.
- Lin, T.-Y., Dollár, P., Girshick, R., He, K., Hariharan, B., and Belongie, S. Feature pyramid networks for object detection, 2017. URL <https://arxiv.org/abs/1612.03144>.
- Liu, P., Orru, Y., Vakil, J., Paxton, C., Shafiullah, N., and Pinto, L. Demonstrating ok-robot: What really matters in integrating open-knowledge models for robotics. In *Robotics: Science and Systems XX*. Robotics: Science and Systems Foundation, July 2024. doi: 10.15607/rss.2024.xx.091. URL <http://dx.doi.org/10.15607/RSS.2024.XX.091>.
- Liu, Y., Wang, T., Zhang, X., and Sun, J. Petr: Position embedding transformation for multi-view 3d object detection, 2022. URL <https://arxiv.org/abs/2203.05625>.
- Liu, Z., Lin, Y., Cao, Y., Hu, H., Wei, Y., Zhang, Z., Lin, S., and Guo, B. Swin transformer: Hierarchical vision transformer using shifted windows, 2021. URL <https://arxiv.org/abs/2103.14030>.
- Luo, J., Fan, W.-C., Wang, L., He, X., Rahman, T., Abolmaesumi, P., and Sigal, L. To sink or not to sink: Visual information pathways in large vision-language models, 2025. URL <https://arxiv.org/abs/2510.08510>.
- Mao, W., Zhong, W., Jiang, Z., Fang, D., Zhang, Z., Lan, Z., Li, H., Jia, F., Wang, T., Fan, H., and Yoshie, O. Robomatrix: A skill-centric hierarchical framework for scalable robot task planning and execution in open-world, 2025. URL <https://arxiv.org/abs/2412.00171>.
- Oquab, M., Darcet, T., Moutakanni, T., Vo, H., Szafraniec, M., Khalidov, V., Fernandez, P., Haziza, D., Massa, F., El-Nouby, A., Assran, M., Ballas, N., Galuba, W., Howes, R., Huang, P.-Y., Li, S.-W., Misra, I., Rabbat, M., Sharma, V., Synnaeve, G., Xu, H., Jegou, H., Mairal, J., Labatut, P., Joulin, A., and Bojanowski, P. Dinov2: Learning robust visual features without supervision, 2024. URL <https://arxiv.org/abs/2304.07193>.
- Qi, C. R., Yi, L., Su, H., and Guibas, L. J. Pointnet++: Deep hierarchical feature learning on point sets in a metric space, 2017. URL <https://arxiv.org/abs/1706.02413>.
- Qiu, R.-Z., Song, Y., Peng, X., Suryadevara, S. A., Yang, G., Liu, M., Ji, M., Jia, C., Yang, R., Zou, X., and Wang, X. Wildlma: Long horizon loco-manipulation in the wild, 2025. URL <https://arxiv.org/abs/2411.15131>.
- Radford, A., Kim, J. W., Hallacy, C., Ramesh, A., Goh, G., Agarwal, S., Sastry, G., Askell, A., Mishkin, P., Clark, J., Krueger, G., and Sutskever, I. Learning transferable visual models from natural language supervision, 2021. URL <https://arxiv.org/abs/2103.00020>.
- Schult, J., Engelmann, F., Hermans, A., Litany, O., Tang, S., and Leibe, B. Mask3d: Mask transformer for 3d semantic instance segmentation, 2023. URL <https://arxiv.org/abs/2210.03105>.
- Shukla, A., Tao, S., and Su, H. Maniskill-hab: A benchmark for low-level manipulation in home rearrangement tasks. In *The Thirteenth International Conference on Learning Representations, ICLR 2025, Singapore, April 24-28, 2025*. OpenReview.net, 2025. URL <https://openreview.net/forum?id=6bKEWevgSd>.
- Su, Y., Zhang, C., Chen, S., Tan, L., Tang, Y., Wang, J., and Liu, X. Dspv2: Improved dense policy for effective and generalizable whole-body mobile manipulation, 2025. URL <https://arxiv.org/abs/2509.16063>.
- Team, O. M., Ghosh, D., Walke, H., Pertsch, K., Black, K., Mees, O., Dasari, S., Hejna, J., Kreiman, T., Xu, C., Luo, J., Tan, Y. L., Chen, L. Y., Sanketi, P., Vuong, Q., Xiao, T., Sadigh, D., Finn, C., and Levine, S. Octo: An open-source generalist robot policy, 2024. URL <https://arxiv.org/abs/2405.12213>.
- Tschannen, M., Gritsenko, A., Wang, X., Naeem, M. F., Alabdulmohsin, I., Parthasarathy, N., Evans, T., Beyer, L., Xia, Y., Mustafa, B., Hénaff, O., Harmsen, J., Steiner, A., and Zhai, X. Siglip 2: Multilingual vision-language encoders with improved semantic understanding, localization, and dense features, 2025. URL <https://arxiv.org/abs/2502.14786>.
- Uppal, S., Agarwal, A., Xiong, H., Shaw, K., and Pathak, D. Spin: Simultaneous perception, interaction and navigation, 2024. URL <https://arxiv.org/abs/2405.07991>.
- Vora, S., Lang, A. H., Helou, B., and Beijbom, O. Pointpainting: Sequential fusion for 3d object detection, 2020. URL <https://arxiv.org/abs/1911.10150>.

- Wu, X., Jiang, L., Wang, P.-S., Liu, Z., Liu, X., Qiao, Y., Ouyang, W., He, T., and Zhao, H. Point transformer v3: Simpler, faster, stronger, 2024. URL <https://arxiv.org/abs/2312.10035>.
- Yan, S., Zhang, Z., Han, M., Wang, Z., Xie, Q., Li, Z., Li, Z., Liu, H., Wang, X., and Zhu, S.-C. M2 diffuser: Diffusion-based trajectory optimization for mobile manipulation in 3d scenes. *IEEE Transactions on Pattern Analysis and Machine Intelligence*, pp. 1–17, 2025. ISSN 1939-3539. doi: 10.1109/tpami.2025.3553454. URL <http://dx.doi.org/10.1109/TPAMI.2025.3553454>.
- Yang, R., Kim, Y., Hendrix, R., Kembhavi, A., Wang, X., and Ehsani, K. Harmonic mobile manipulation, 2024. URL <https://arxiv.org/abs/2312.06639>.
- Ze, Y., Zhang, G., Zhang, K., Hu, C., Wang, M., and Xu, H. 3d diffusion policy: Generalizable visuomotor policy learning via simple 3d representations. In *Proceedings of Robotics: Science and Systems (RSS)*, 2024.
- Zhao, H., Shi, J., Qi, X., Wang, X., and Jia, J. Pyramid scene parsing network, 2017. URL <https://arxiv.org/abs/1612.01105>.
- Zhao, T. Z., Kumar, V., Levine, S., and Finn, C. Learning fine-grained bimanual manipulation with low-cost hardware, 2023. URL <https://arxiv.org/abs/2304.13705>.

A. Details of ManiSkill-HAB Experiments.

Robot Configuration. We use the Fetch mobile manipulation robot as the agent. The robot is equipped with a 7-DoF manipulator, a vertically actuated torso, and a 2-DoF differential-drive mobile base.

Action Space. The agent’s action space is a 13-dimensional continuous vector. Among these, 11 dimensions control joint position increments of the manipulator, torso, and head via PD joint controllers, while the remaining 2 dimensions control the linear and angular velocities of the mobile base. All action commands are normalized to the range $[-1, 1]$.

Training Dataset. We collect training data in ManiSkill-HAB using reinforcement learning algorithms. Specifically, PPO is used to collect trajectories for the open and close tasks, while SAC is used for the pick and place tasks. For each task, we collect 1,000 successful trajectories.

Training Protocol. For all methods, we train each task on 1,000 trajectories for 100k training steps, using a batch size of 64, and report the task success rate as the evaluation metric. Table 5 presents the hyperparameters used to train our method.

Table 5. Training hyperparameters.

Hyperparameter	Value
Optimizer Type	<i>Adam</i>
Batch Size	64
Learning Rate	1×10^{-4}
Learning Rate Warm Up Steps	1000
Learning Rate Cosine Decay Steps	100,000
λ_{ent}	0.1
λ_{scale}	1
λ_{align}	0.01

Visualization of Task Execution Trajectories. Figures 5 and 6 visualize the execution trajectories of InCoM across multiple representative tasks.



Figure 5. Execution trajectories of our method across four TidyHouse and PrepareGroceries tasks.

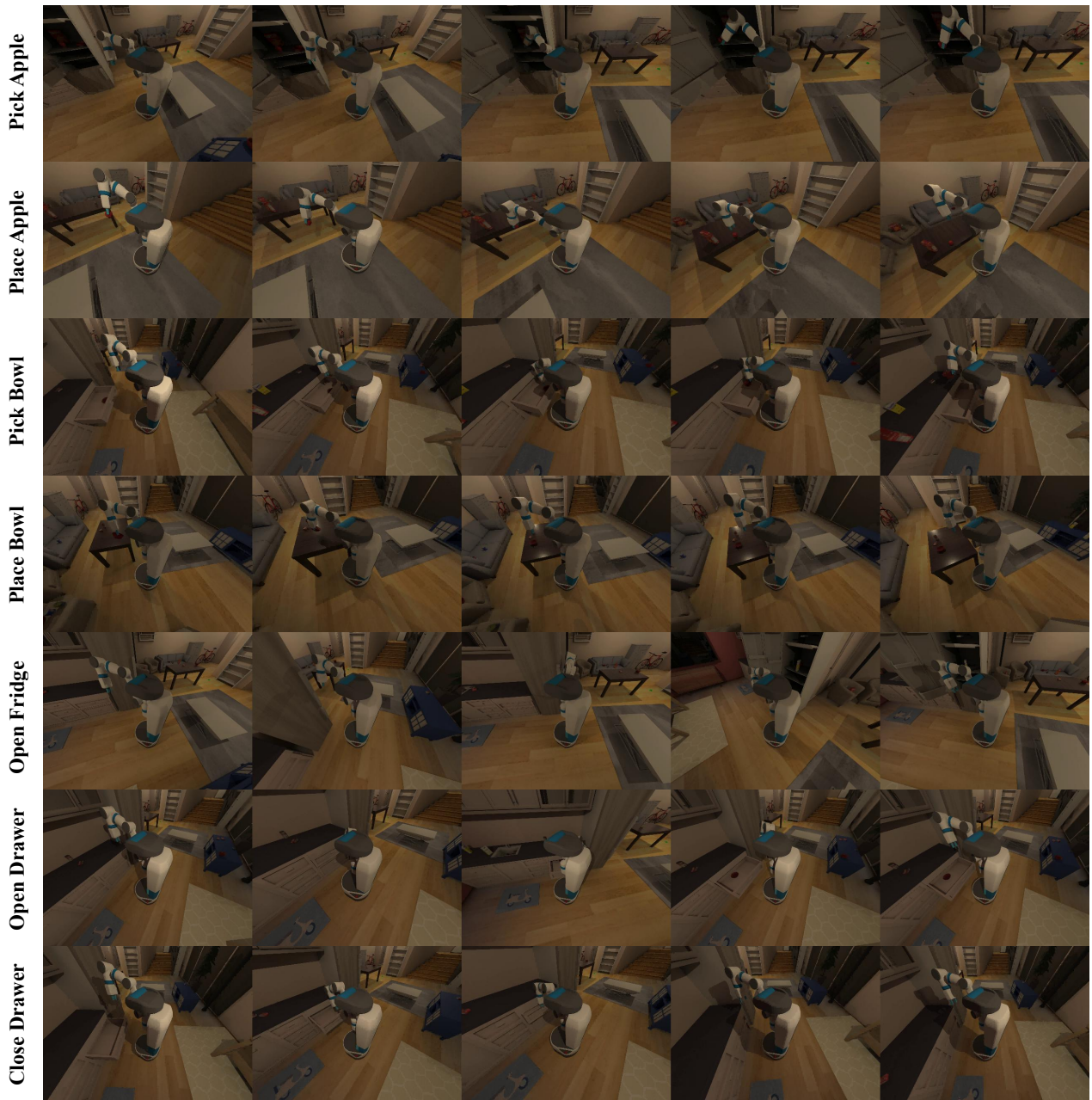


Figure 6. Execution trajectories of our method across seven SetTable tasks.

Analysis of Pretrained Model Baseline Results. As shown in Table 6, we additionally compare InCoM with π_0 (Black et al., 2024), a large-scale pretrained policy. Unlike InCoM and other baselines evaluated in the main paper, which are trained from scratch under the same settings, π_0 relies on extensive pretraining on large-scale datasets. To avoid confounding the main comparison, we report this result separately. Despite its pretraining advantage, π_0 underperforms InCoM, likely due to its decoder design being less suited for whole-body coordination and its reliance on RGB-only observations.

Comparative Analysis of Execution Trajectories. We conduct a qualitative comparison of the execution trajectories of ACT, π_0 , and InCoM on the Pick Apple and Open Drawer tasks, as shown in Fig. 7. In the Pick Apple task, ACT fails to effectively avoid the internal shelf inside the fridge due to limited perceptual capability, causing the manipulator to be repeatedly obstructed when approaching the target and preventing successful insertion into the fridge for grasping. π_0 manages to bypass the shelf, but fails to accurately localize the apple during the final interaction stage; as a result, the

Table 6. Comparison of task success rates between π_0 and InCoM on the SetTable scenario in the ManiSkill-HAB benchmark.

Method	Pick Apple	Place Apple	Open Fridge	Pick Bowl	Place Bowl	Open Drawer	Close Drawer	Mean
π_0 (Black et al., 2024)	29	53	90	27	58	74	88	59.9
InCoM(Ours)	59.4	84.1	87.3	84.1	82.5	88.9	100	83.8

manipulator inadvertently pushes the apple toward the back of the fridge, leading to object drop and task failure. In contrast, InCoM is able to plan a reasonable manipulator trajectory under occlusion, precisely deliver the end-effector to the target region, and successfully grasp the apple. In the Open Drawer task, ACT exhibits insufficient coordination between the mobile base and the manipulator during the pulling motion. The base fails to appropriately support the arm movement, resulting in the drawer being opened only slightly. π_0 suffers from a similar issue in its first attempt, but eventually completes the task after a second adjustment. By comparison, InCoM opens the drawer in a single, continuous, and coordinated motion, demonstrating more stable and efficient base–arm coordination.

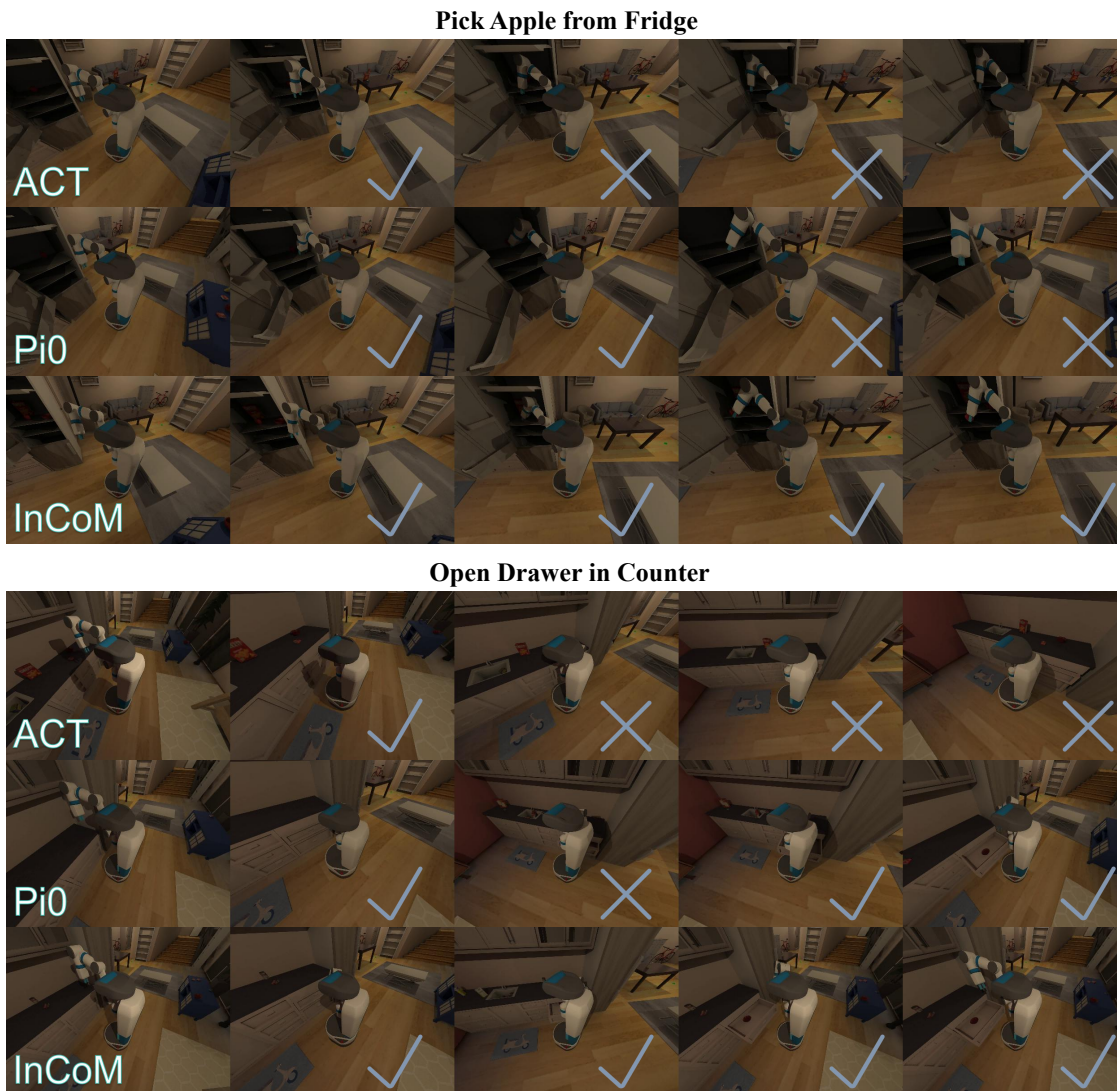


Figure 7. Visualization of execution trajectories for ACT, π_0 , and InCoM on the Pick Apple and Open Drawer tasks.

Failure Case Analysis of InCoM. We report several representative failure cases in Fig. 8 to illustrate the current limitations of InCoM under challenging initial conditions and physical interactions. **(1) Target out of view due to initial placement.** In the task of picking an apple from the fridge, the robot was initialized at a lateral position relative to the fridge. As a result, the

target object was not visible in the initial observations, preventing the policy from establishing a reliable perception–action plan and leading to task failure. **(2) Object instability at evaluation start.** In the task of picking a can from a table, the can was randomly spawned at an extreme edge of the tabletop. The object fell off immediately at the beginning of evaluation due to gravity, before any meaningful interaction could take place, resulting in an unavoidable failure. **(3) Inaccurate size estimation during placement.** In the task of placing a box onto a countertop, the box instance was significantly larger than those commonly seen during training. The policy appeared to underestimate the object’s spatial extent, causing the box to collide with the countertop edge during placement and subsequently fall. **(4) Unstable grasp with partial recovery.** In the task of grasping a box from a sofa, the initial grasp was unstable and the box slipped from the gripper onto the floor. However, the robot was able to subsequently re-detect the fallen object and successfully pick it up from the ground, demonstrating partial recovery capability despite the initial failure.

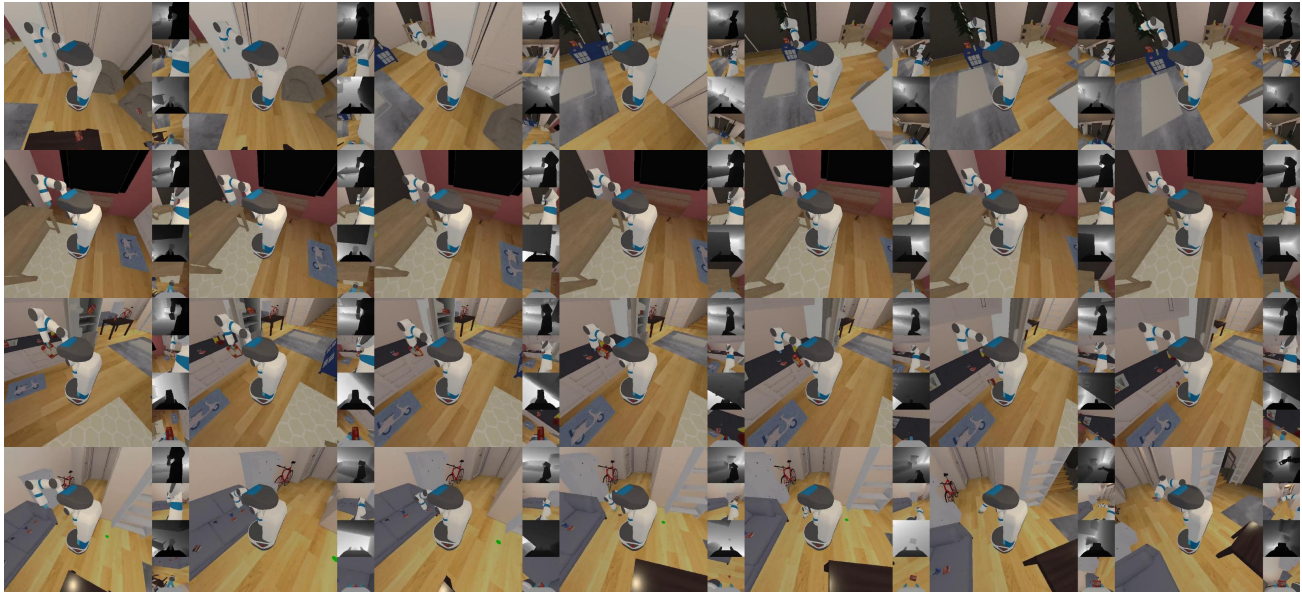


Figure 8. **Representative failure cases of InCoM.** From top to bottom, the robot performs: picking an apple from a fridge, picking a can from a table, placing a box onto a countertop, and picking a box from a sofa.

B. Visualization Analysis of Feature Receptive Field and Multi-scale Spatial Attention

To further investigate how the image encoder in InCoM processes features at different network depths, we conducted a visualization analysis of its receptive fields. Specifically, we applied a patch-to-patch attention analysis method, selecting five representative spatial locations in the input image as query patches to examine how attention is distributed across the multi-scale feature hierarchy. The selected query patches include the geometric center of the image and four positions near the corners while avoiding the image boundaries, minimizing potential edge effects inherent to the Vision Transformer architecture. The visualization is presented as a 3×5 heatmap matrix, with rows corresponding to different encoder layers (shallow, mid, and deep from top to bottom) and columns representing the five query patches. White hollow circles indicate the centers of the query patches, and the heatmap color reflects attention strength, with red regions corresponding to areas contributing most to the query patch.

As shown in Fig. 9, the attention maps reveal a clear hierarchy in spatial modeling across different depths. In shallow layers, attention is concentrated around the query patch, indicating strong locality and a focus on capturing fine-grained details. In mid layers, attention gradually expands to cover larger contextual regions related to the query, demonstrating the model’s capacity to capture broader scene context. In deep layers, attention extends even further, forming a pronounced global receptive field and enabling the integration of information across the entire scene. It is worth noting that a persistent high-response region in the upper-left corner of the deep-layer heatmaps corresponds to the commonly observed “Attention Sink” in Vision Transformers (Darcet et al., 2024; Gu et al., 2025; Luo et al., 2025), which serves as a global register for storing scene-level information and does not interfere with perception of actual physical targets. Because the Attention Sink absorbs a fixed proportion of absolute attention weights, the attention assigned to actual physical targets and surrounding

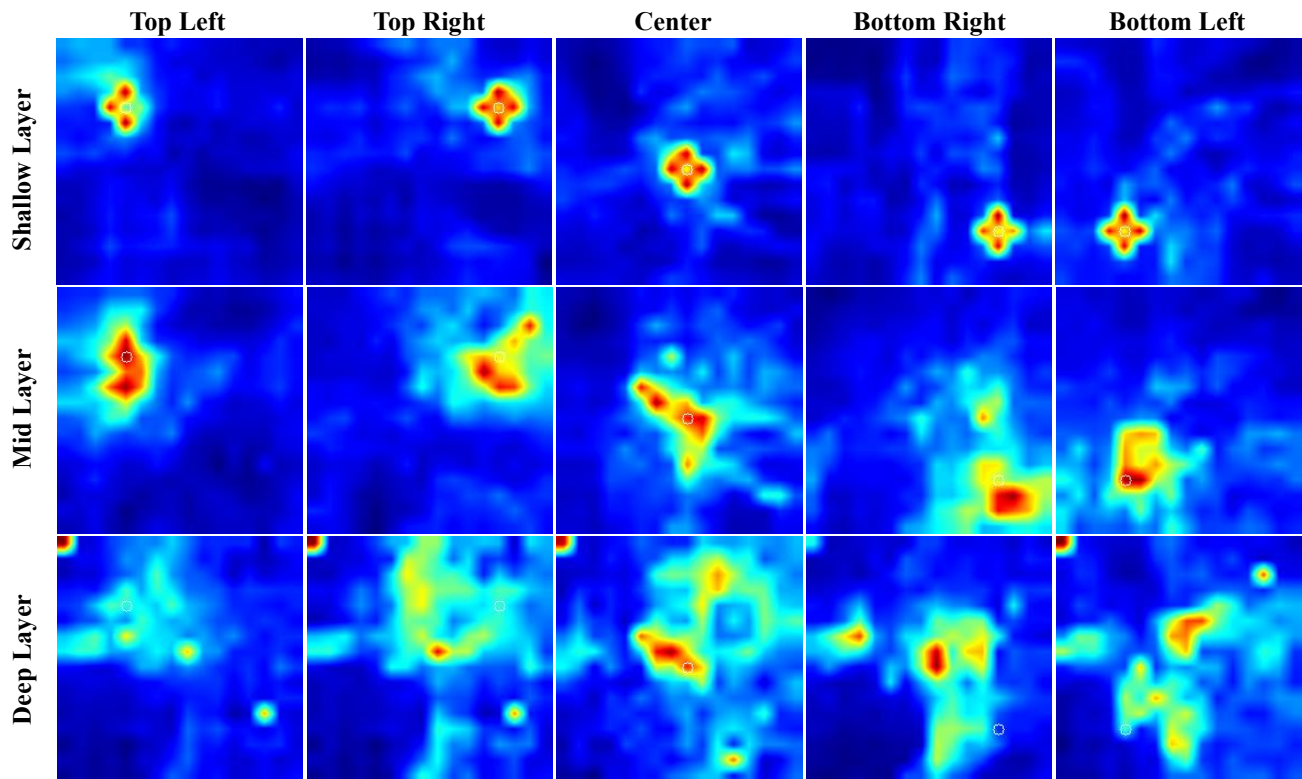


Figure 9. Visualization of patch-to-patch attention across network depths in InCoM. Each row corresponds to a different encoder layer (shallow, mid, deep), and each column shows one of five representative query patches. White hollow circles indicate query patch centers, and the heatmap color represents attention strength. Shallow features focus on local details, mid-layer features capture broader context, and deep features integrate global scene information, forming a multi-scale perceptual hierarchy.

background appears relatively smaller; during linear normalization of the heatmaps, these low-amplitude but semantically rich responses are visually suppressed, making the deep-layer receptive field appear narrower than it truly is. In reality, deep features implicitly encompass a broader and more coherent spatial representation.

Overall, this visualization analysis demonstrates that the image encoder used in InCoM produces complementary representations at different depths: shallow features retain high-resolution local details, while deep features provide high-level semantic information with global scene context. This multi-scale feature modeling establishes a stable and rich perceptual foundation for subsequent intent-driven modulation and coordinated whole-body action generation.